nature communications

Article

https://doi.org/10.1038/s41467-024-54856-0

Atlantic Ocean thermal forcing of Central American rainfall over 140,000 years

Received: 2 July 2024

Accepted: 20 November 2024

Published online: 04 December 2024

Check for updates

Giuseppe Lucia[1], Davide Zanchettin[2], Amos Winter[3], Hai Cheng[4], Angelo Rubino[2], Osmín J. Vásquez[5], Juan Pablo Bernal[6], Mario Cu-Xi[7] & Matthew S. Lachniet[1]

Tropical hydroclimate in monsoonal regions has been largely understood according to the orbital monsoon hypothesis, in which rainfall exhibits strong covariation with local summer insolation on precessional (~21,000 years) time scales, as exemplified in the Asian and South American monsoon stalagmite records. However, paleo-rainfall variations in some tropical regions are poorly explained by the orbital hypothesis, suggesting alternative forcing mechanisms of regional monsoon changes. Here, we show a 140,000-year record of Central American rainfall from oxygen-isotope ($\delta^{18}O$) time series of precisely dated stalagmites which reveals two dominant thermally-controlled monsoon regimes in which the Atlantic Ocean thermal state linked to the meridional overturning circulation (AMOC) is the primary driver, and local orbital summer insolation control is limited. Our reconstruction, supported by isotope-enabled climate model simulations, pinpoints the potential impacts of future AMOC weakening on the Central American and Caribbean climate.

The orbital monsoon hypothesis predicts that local summer insolation on precessional time scales drives monsoon circulation, for example by heating the large Asian and South American landmasses[1]. Superimposed on precessional-scale rainfall variations in these regions are anti-phased abrupt monsoon events linked to ice-rafted debris deposition in the North Atlantic Ocean called Heinrich events, and associated with monsoon weakening in Asia[2] and strengthening in South America[3], as revealed by cave calcite $\delta^{18}O$. In the tropics, changing rainfall amounts and oxygen-isotope composition ($\delta^{18}O_p$) have been attributed both to changes in local summer insolation that influence atmospheric circulation and to latitudinal shifts in the Intertropical Convergence Zone (ITCZ), which favors the warmer hemisphere[4]. Such coherent antiphasing of rainfall characterizes a unified circulation system known as the Global Monsoon[5,6]. However, rainfall variations in some major tropical regions, notably in Central America and the Caribbean[7–9], eastern Mexico[10], and other regions[11], lack a clear precessional scale forcing, possibly because of their smaller continental area relative to surrounding oceans hampered large-scale land-sea thermal gradients (typical of classic monsoon systems), or because of a stronger ocean control on atmospheric dynamics.

Testing for alternative hypotheses on primary drivers of rainfall variations, such as Atlantic Ocean temperature or dynamics[12] requires hydroclimate reconstructions near the tropical North Atlantic Ocean, a key center of action for abrupt climate change[13]. For example, a strong coupling between millennial-scale climate variability recorded in marine sediments of the Cariaco Basin off northern South America and similar events in Greenland ice cores demonstrates a strong coupling between high and low latitude climate in the Atlantic/Caribbean region[14,15]. However, variations in the strength of tropical convection over and upwind of Central America may not behave similarly to the Cariaco Basin, particularly as Central America is outside the core oceanic region of the ITCZ and responds to more complex ocean-atmosphere dynamics other than solely north-south ITCZ latitudinal changes. Thus, precisely-dated paleoclimate records from continental

[1]Department of Geoscience, University of Nevada Las Vegas, Las Vegas, NV, USA. [2]Department of Environmental Sciences, Informatics and Statistics, University Ca' Foscari of Venice, Mestre, Italy. [3]Department of Earth and Environmental Systems, Indiana State University, Terre Haute, IN, USA. [4]School of Human Settlement and Civil Engineering, Xi'an Jiaotong University, Xi'an, China. [5]Centro Universitario del Norte, Universidad de San Carlos de Guatemala, Cobán, Guatemala. [6]Instituto de Geociencias, Universidad Nacional Autónoma de México, Juriquilla, Querétaro, México. [7]Instituto Nacional de Sismología, Vulcanología, Meteorología e Hidrología, Guatemala City, Guatemala. e-mail: Matthew.Lachniet@unlv.edu

locations north of 10 °N would provide key information on the temporal and dynamical response of Central American regional monsoon to Atlantic Ocean forcing.

The Atlantic meridional Overturning circulation (AMOC) is one of the core tipping elements of the Earth's climate system[16] capable of triggering far-reaching, potentially irreversible global changes. Paleoclimate evidence documents rapid transitions between stable circulation modes of AMOC throughout the last glacial cycle[17]: a strong (interglacial) mode in which warm surface waters are transported to the northern high latitudes, release heat to the atmosphere, cool and sink at depths to form deep water masses moving southward (North Atlantic Deep Water formation); and a weak (glacial) circulation mode where northward heat transport is reduced, oceanic convection is shallower, and heat accumulates in the tropics. Tropical hydroclimate reconstructions have shown that changes between AMOC states cause shifts in the latitudinal position of the rain belt and the intensity of monsoon precipitation[18]. Presently, AMOC transports heat from the tropics to the northern hemisphere high latitudes via the Gulf Stream, contributing to a northern mean position of the tropical rainbelt[19,20]. Current state-of-the-art climate models project future AMOC weakening in response to greenhouse gas warming[21], albeit with widespread inter-model discrepancy regarding magnitude and rate of slowdown[22]. For associated impacts, key uncertainties are the role of AMOC on past and future tropical rainfall variability[4,23] and the regions most sensitive to future AMOC decline[22,24,25].

Central America is an ideal location to test for AMOC-tropical climate controls because it is teleconnected to the AMOC upper limb via the northeasterly trade winds, downwind of the large heat reservoirs of the tropical North Atlantic, Caribbean Sea, and Gulf of Mexico (the broader Atlantic Warm Poo[7,26]). The rainfall annual cycle responds to interactions between regional SST, ITCZ latitudinal changes, and near-surface wind dynamics, primarily northeasterlies and the Caribbean Low-Level Jet (CLLJ), linked to east-west excursions of the North Atlantic Subtropical High (NASH)[27–29]. About ~65% of the 2500 mm of our site's annual rainfall[30] occurs during the May through November wet season when SSTs exceed 27.5 °C, the Atlantic Warm Pool is at its maximum areal extension[31], and a weaker CLLJ over the Caribbean contributes to deep convective systems. During winter (December-April), an intensified CLLJ linked to the westward expansion of NASH and lower SST increases atmospheric subsidence over the Caribbean suppressing regional convection[27]. Winter rainfall, which accounts for ca. 35% of the annual total precipitation, consists mostly of localized convection and northerly-sourced (*nortes)* air masses. We refer to the strong seasonality of Central American rainfall as part of the Global 'monsoon', while recognizing that the region lacks some of the distinguishing features of classic monsoon circulation such as large-scale wind reversals.

Here, we show from a speleothem-based paleo-rainfall record over the last glacial cycle (140,000 years to present) from Guatemala that the Atlantic Ocean overturning circulation (AMOC) and sea surface temperature (SST) drive Central American hydroclimate variations and propose a strong link between AMOC and monsoon strength. This thermally-driven Central American monsoon is distinct from precession-driven monsoon systems elsewhere in the tropics, and highlights the direct forcing of Atlantic Ocean thermal states on Central American regional climate.

Results and Discussion

Glacial-interglacial monsoon convective states

We reconstruct Central American hydroclimate from calcite $\delta^{18}O$ time series of precisely dated speleothems from three Maya highland caves at ~15°N latitude on the Caribbean slope of Guatemala (Supplementary Fig. 1), Grutas del Rey Marcos (RM)[12], Cueva Jul Iq (JQ), and Cueva Bombil Pek (BO). Our reconstruction is anchored by ninety-three ^{230}Th radiometric ages on nine replicating stalagmites to produce a composite time series, which was adjusted for inter-cave differences (related to the elevation difference between caves sites) and for the ice-volume corrected seawater isotopic composition ($\delta^{18}O_{ivc}$, in ‰ Vienna Pee Dee Belemnite, VPDB throughout)[32] (Supplementary Fig. 2; Methods). We interpret $\delta^{18}O_{ivc}$ as primarily a proxy for $\delta^{18}O$ of precipitation ($\delta^{18}O_p$) reaching the cave site, which in turn is controlled by rainfall amount along the prevailing source-to-cave moisture trajectory[33].

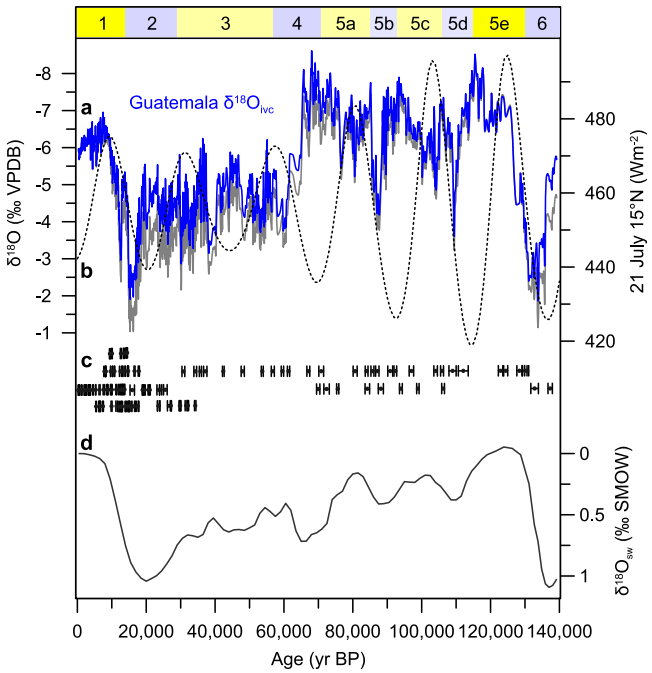

Fig. 1 | Central American monsoon reconstruction over the last glacial cycle. **a** Composite Guatemala speleothem ice-volume corrected (blue) and measured (grey) $\delta^{18}O$. **b** July 21 insolation curve (dotted) at 15°N (ref. 91). **c** U-series ages with associated 2σ uncertainty of nine stalagmites. **d** Ocean $\delta^{18}O$ from ref. 32, used to adjust our $\delta^{18}O$ record for ice-volume changes ($\delta^{18}O_{ivc}$). Cold (blue) and warm (yellow) Marine Isotope Stages (MIS 1-6) are shown.

At our cave sites, lower monthly $\delta^{18}O_p$ values are associated with enhanced rainfall from deep convection during May-November ($r = -0.68$, $p < 0.0001$; Supplementary Fig. 3, 4). Although seasonal changes of the ITCZ latitudinal position modulate regional moisture convergence across tropical America, today the ITCZ does not reach the latitude of our cave sites (15 °N) during boreal summer[7]. Rather, a broad zone of convection persists over Central America north of the oceanic ITCZ. We thus discuss $\delta^{18}O$ variations in our record in terms of regional convective intensity to distinguish it from proxy records from lower latitudes, such as the Cariaco Basin[15] (10 °N), that are more directly affected by north-south ITCZ changes. Cave drip waters integrate amount-weighted precipitation $\delta^{18}O$ values, thus lower $\delta^{18}O$ indicates more regional convection and a stronger monsoon and higher $\delta^{18}O$ reflecting less convection (Supplementary Fig. 5). Our study sites are particularly sensitive to tropical North Atlantic processes (Supplementary Fig. 6) because ~75% of the annual precipitation originates in the Caribbean/western tropical Atlantic region[34], with smaller contributions from northern extra-tropical cold-fronts (~15%) and eastern tropical Pacific (~10%).

Central American paleoclimate is defined by a distinct bi-modal glacial-interglacial topology over the last 140,000 years (Fig. 1), suggesting the existence of two primary convective regimes: a weak glacial monsoon and a strong interglacial monsoon, either of which may be interrupted by even more extreme abrupt episodes of monsoon weakening. The prolonged strong monsoon between MIS 5e and the

https://doi.org/10.1038/s41467-024-54856-0

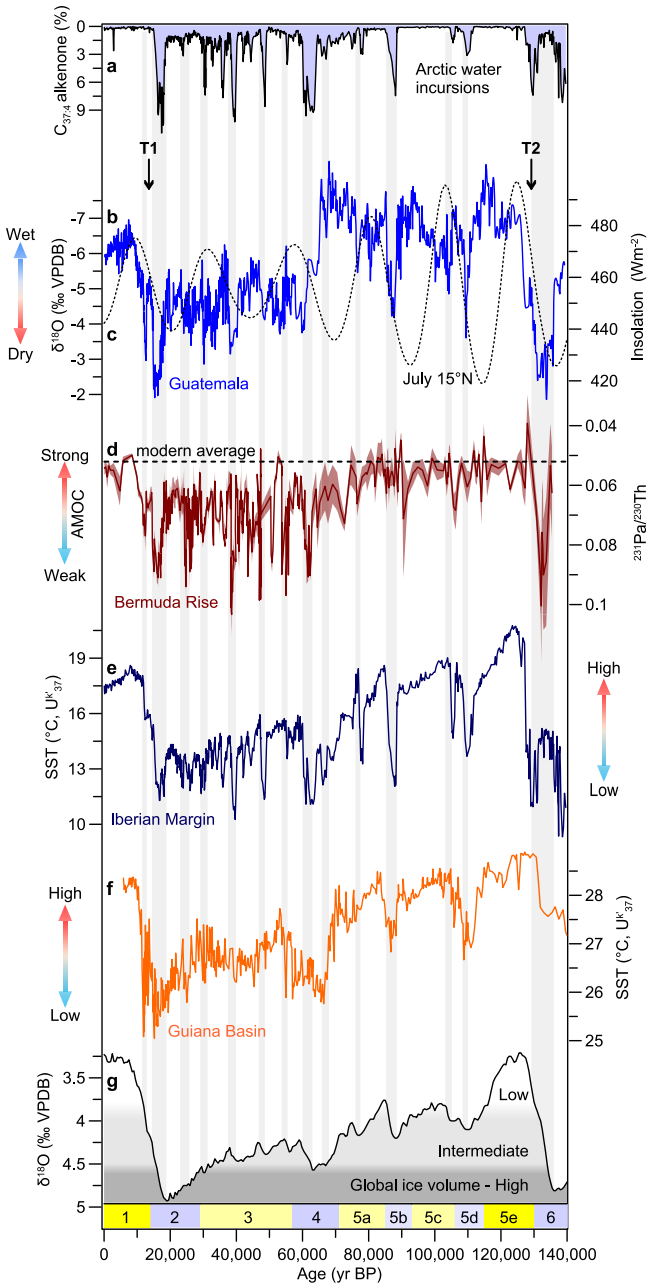

Fig. 2 | Atlantic Ocean temperature and circulation control on Central American monsoon variation. a Alkenone ratio $C_{37:4}$, a proxy for Arctic surface waters reaching the subtropical North Atlantic[36]. **b** Guatemala $\delta^{18}O_{ivc}$ record (this study); **c** July 21 insolation curve at 15°N (ref. 91). **d** $^{231}Pa/^{230}Th$, a proxy for the strength of the Atlantic Meridional Overturning Circulation (AMOC)[13,17,45]. **e** Alkenone based sea surface temperature (SST) from off the Iberian margin[36]. **f** Alkenone based SST from the tropical Guiana Basin (digitized)[39]. **g** Global ice volume from benthic $\delta^{18}O_c$ (ref. 42). Glacial termination I (T1) and II (T2) are also highlighted. Vertical grey bars denote Heinrich stadials (HS0-11). Marine Isotope Stages (MIS 1-6) are also shown.

first half of MIS 4 lasted more than 60,000 years and was punctuated by several millennial-scale weak monsoon events.

Following ice age terminations I and II (T1 and T2 in Fig. 2), peak monsoon strength was delayed for several thousand years behind minimum global ice volume, peaking at ca. 125,500 yr BP and 9000 yr BP, respectively, and in both cases relatively stable and wet conditions were maintained for several millennia. A large and abrupt transition to a glacial weak monsoon state occurred between 66,000 and 60,000 yr BP, contemporaneously to intensified iceberg discharges in the North Atlantic[35,36] and to an abrupt AMOC slowdown[17] (Fig. 2).

Our observations reveal that convective intensity was decoupled from orbital precession during the last glacial/interglacial cycle (Fig. 1a, b): wet intervals lasted longer than a precessional cycle and spanned insolation lows, whereas dry intervals were commonly shorter than a full precessional cycle. Thus, a strong glacial-interglacial cycle distinguishes Central America from monsoons in Asia[2], South America[37], and Borneo[38] that are more clearly paced by precession and local summer insolation (Supplementary Fig. 7).

AMOC and SST forcing

Comparisons with North Atlantic paleoceanographic reconstructions[17,36,39] show that Central American monsoon intensity is primarily responding to tropical and subtropical North Atlantic SST and AMOC strength, with superimposed millennial-scale monsoon collapses during cold North Atlantic Heinrich stadials (Fig. 2). For example, SST records from the Iberian Margin[36] and the Guiana Basin[39] off northern South America show a thermal structure similar to our rainfall record, with a prolonged last interglacial period punctuated by millennial scale cooling and drying excursions. The peak warming off Iberia at 127,100 yr BP (Fig. 2e) closely overlaps the resumption of strong convection over Central America but is delayed behind the ca. 130,000 yr BP global ice volume minimum.

Three major weak monsoon intervals (high $\delta^{18}O_{ivc}$) coincided with Arctic water penetration to the subtropics during MIS 5 as inferred from high $C_{37:4}$ alkenone ratios in marine sediments, at 111,500 to 107,500 yr BP (MIS 5 d), 105,600 to 103,600 yr BP (MIS 5c), and 89,000 to 85,000 yr BP (MIS 5b) (Fig. 2a). These monsoon collapses coincide with a period of moderate to low global ice volume (Fig. 2g), suggesting that during relatively warm conditions, Central American rainfall lies close to a tipping point in which slight cooling may produce extensive monsoon suppression.

Further, we show that millennial-scale weak monsoon periods over the last glacial/interglacial cycle were synchronous within dating uncertainties to cooling episodes in the northern high- and mid-latitudes[36,40] related to ice-rafted debris (IRD) deposition and melt-water routing to the North Atlantic Ocean, called Heinrich (H) events or stadials (HS)[35,41]. For instance, the weakest monsoon convection in Central America just prior to Terminations II and I are coeval to the largest North Atlantic HS11 and HS1, while the abrupt dry phases at the MIS 5b and MIS 5 d coincide with HS8 and HS10 (Ref. 42; Fig. 2). Less severe monsoon weakenings are also recorded in the Guatemalan stalagmites throughout both warm MIS 5 and cold stages MIS 4-2. Although our monsoon reconstruction shares Heinrich dry events with the Cariaco Basin, our data lack the distinct millennial-scale Dansgaard–Oeschger (DO) variability evident in the Greenland ice core $\delta^{18}O$[43] and Cariaco Basin records[15]. These differences, along with the stronger correspondence between our record and Atlantic SST, suggest that Central American monsoon strength is responding to different forcings than those inferred from the marine sediments in the Cariaco Basin and has a unique paleoclimatic history separate from the southern Caribbean[15,44].

Remarkably, the Central American monsoon responded on a one-to-one basis (Fig. 3) with AMOC over the last deglaciation, as detailed in the $^{231}Pa/^{230}Th$ ratios in Bermuda rise ocean sediments[17,45] in the subtropical North Atlantic. Our record indicates moderate monsoon strength at the Last Glacial Maximum (LGM, ca. 20,000 to 18,000 yr BP in our record), a monsoon collapse at 17,500 to 14,800 yr BP (HS1), a return to wetter conditions during the Bølling-Allerød (B-A, 14,800 to 12,800 yr BP), another monsoon weakening during the Younger Dryas (YD, 12,800 to 11,600 yr BP), and a gradual monsoon strengthening in the Early Holocene to reach near-modern values by 9000 yr BP[12]. Each of these weak monsoon periods was associated with cooling and AMOC slowdowns, and vice versa for strong monsoon intervals. The

https://doi.org/10.1038/s41467-024-54856-0

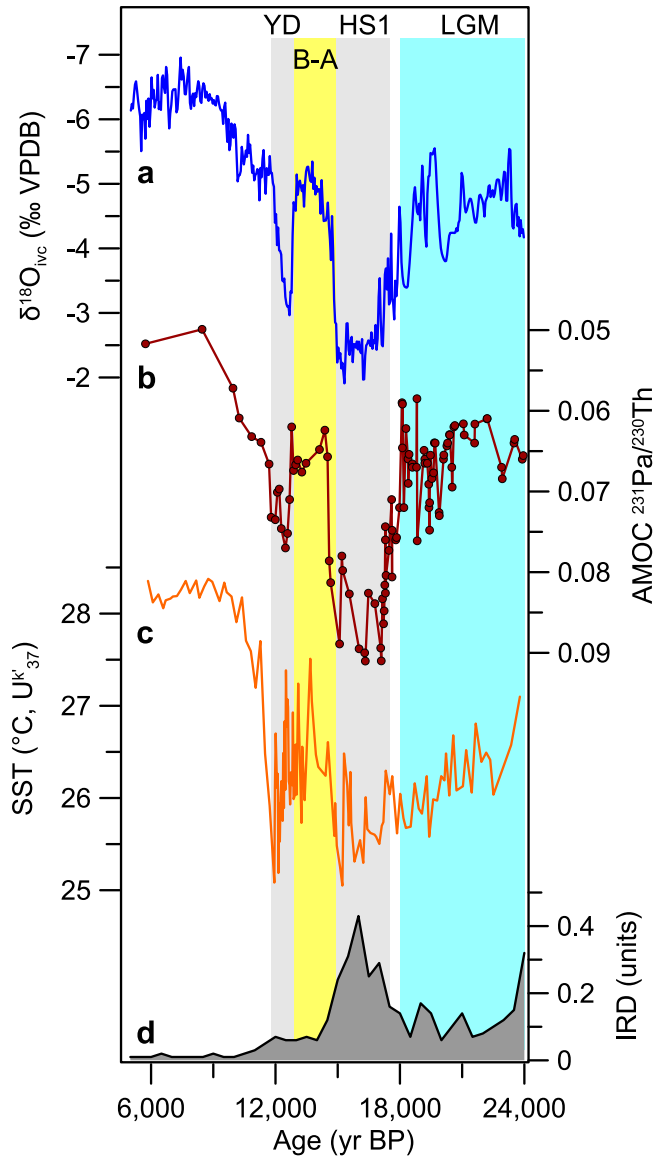

Fig. 3 | Central American monsoon evolution shows a one-to-one coupling with AMOC and SST over Termination 1. a Guatemala $\delta^{18}O_{ivc}$ record (this study); **b** $^{231}Pa/^{230}Th$ ratios in subtropical North Atlantic sediments[45]. **c**, Alkenone-based SST reconstruction from the Guiana Basin off northern South America (digitized)[39]. **d** Ice-rafted debris (IRD) stack for the North Atlantic Ocean[42]. Vertical bars denote: Younger Dryas (YD), Bølling-Allerød (B-A), Heinrich Stadial 1 (HS1), and Last Glacial Maximum (LGM).

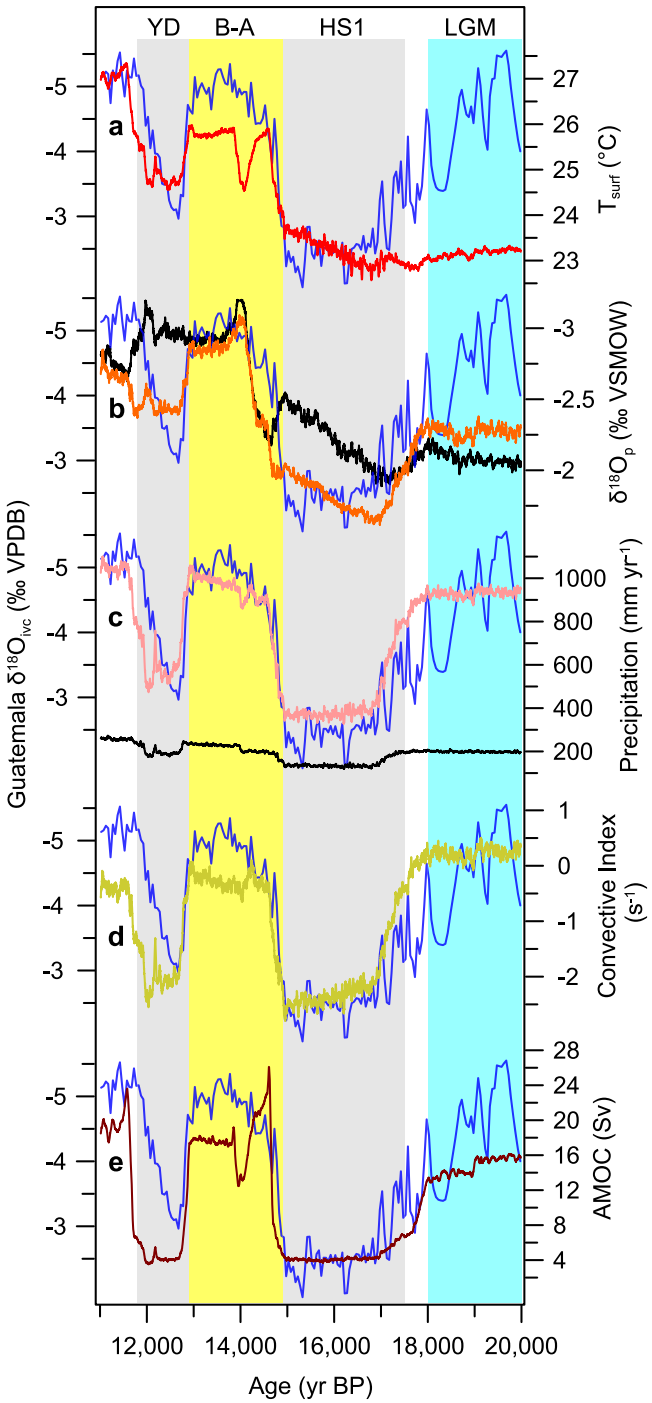

Fig. 4 | Guatemala $\delta^{18}O_{ivc}$ versus iTRACE model output. The Guatemala reconstruction is shown in blue, and iTRACE[47] output (**a**-**e**) for Central American and the Caribbean (latitudes 10.42° to 21.78° and longitudes 265° to 300°) as 31-yr running averages. **a** iTRACE simulated surface temperature. **b** iTRACE $\delta^{18}O_p$ for MJJASON (orange) and DJFMA (black). **c** Rainfall amount for MJJASON (pink) and DJFMA (black). **d** Convective activity index for MJJASON. **e** Simulated AMOC from the equator to 49.6°N from the 500 to 1200 m depth. The iTRACE model accurately simulates the $\delta^{18}O_p$ response to changing regional rainfall amount in Central America and the Caribbean, which is explained by changes in surface temperature related to AMOC strength. Vertical bars define Younger Dryas (YD), Bølling-Allerød (B-A), Heinrich 1 (HS1), and Last Glacial Maximum (LGM).

moderate monsoon during the LGM is linked to similarly moderate AMOC strength comparable to that during the B-A, and provides evidence for an active – though weaker than modern – monsoon during the Last Glacial Maximum in Guatemala. Reconciling this observation with proxy data indicating a strong LGM monsoon elsewhere in the neotropics is an important target for future work[7,46].

Model constraints on AMOC-monsoon link

We use iTRACE[47] data – an ensemble of transient isotope-enabled simulations based on the CESM v1.3 and spanning 20,000 to 11,000 yr BP - to demonstrate that during the last deglaciation the strength of the Central American monsoon can be explained by synchronous changes in simulated $\delta^{18}O_p$, convective intensity, and AMOC strength (Fig. 4). For instance, the iTRACE full forcing experiment (including ice sheet, greenhouse gas, orbital, and meltwater forcing) shows that an increase in speleothem $\delta^{18}O_{ivc}$ coincides with decreases in AMOC strength, North Atlantic surface temperature, and regional convective rainfall and a convective activity index in Central America and Caribbean (see Methods for details). Simulated $\delta^{18}O_p$ values increase

https://doi.org/10.1038/s41467-024-54856-0

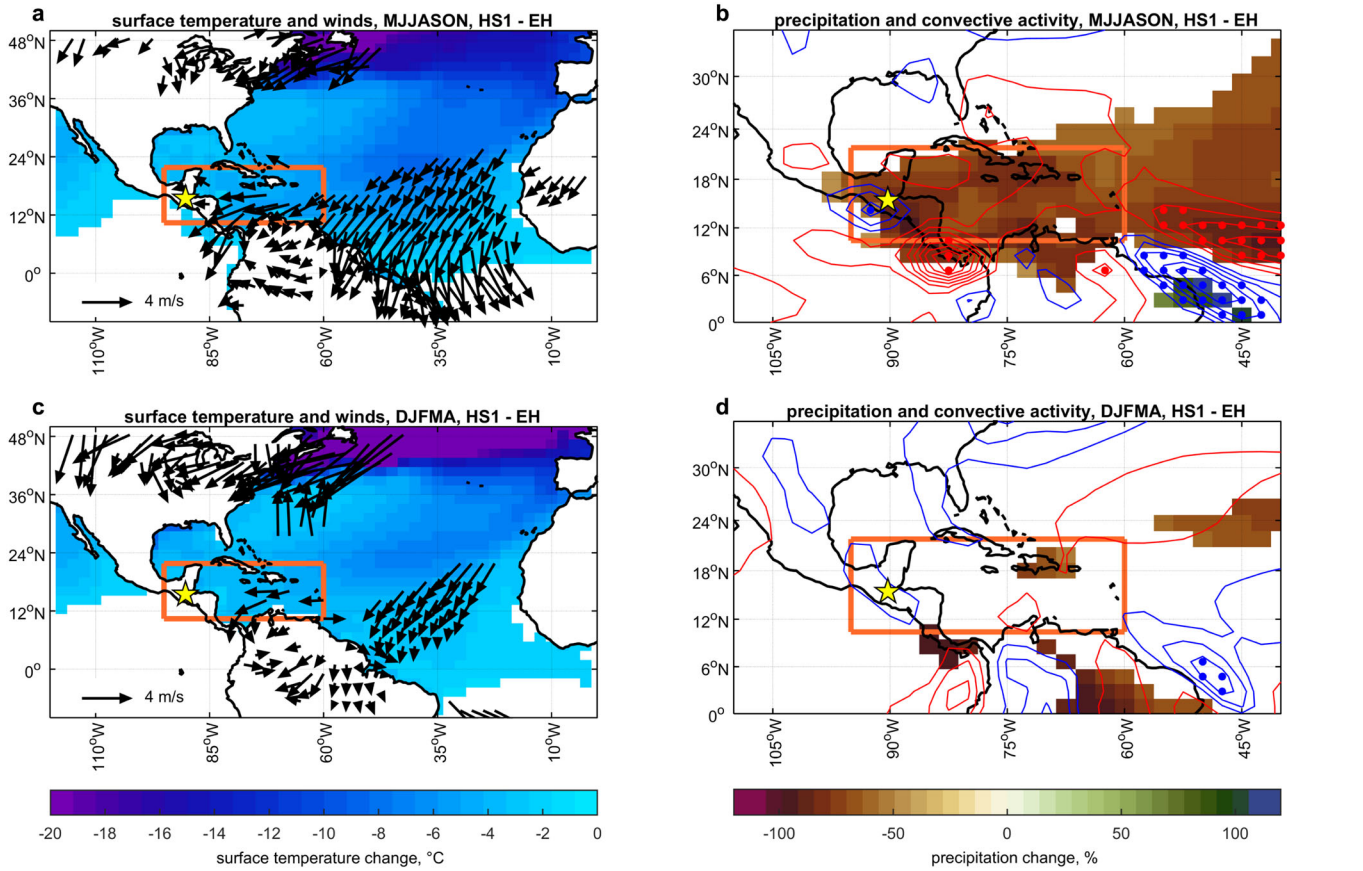

Fig. 5 | iTRACE simulations for Heinrich Stadial 1 (15,200–16,800 yr BP) minus the Early Holocene (11,001–11,500 yr BP) show Caribbean/Tropical Atlantic SST cooling and wet season rainfall reductions related to AMOC weakening. **a** May-November difference in surface temperature (colors) and near-surface winds (arrows). **b** Difference in wet season Central American rainfall (shading as percentage changes relative to the Heinrich Stadial 1 climatology) was associated with a weakened atmospheric convective activity. **c**-**d** Same as **a** and **b** but for the dry (December to April) season. Surface temperature, wind vector, and precipitation anomalies are shown where significant (0.01 level); the difference in convective activity is shown full field (blue: positive; red: negative; shown at 2 s^{-1} intervals), with dots indicating significant differences within 1-99 percentile range. Maps are plotted with the M_map package[92] for MATLAB software, using the Global Self-consistent, Hierarchical, High-resolution Geography Database (GSHHG)[93] for coastlines.

during HS1 and the YD, almost perfectly matching the speleothem $\delta^{18}O_{ivc}$ and weak convective intervals (Figs. 4b and d).

The iTRACE simulation shows that during HS1 rainfall was suppressed from Central America east to the Caribbean Sea, coupled with a general weakening of convective activity over the North Atlantic (Figs. 5b and d). The rainfall reduction is clearly linked to Caribbean SST cooling of ~5 °C associated with meltwater influx to the North Atlantic and a pronounced slowdown of the AMOC. The strongest iTRACE precipitation response is seen in the May through November wet season, while weaker for winter (DJFMA) rainfall (Fig. 4c). The eastern tropical Pacific Ocean was not an important moisture source, in agreement with modern moisture back-trajectory analyses (Supplementary Fig. 6). SST cooling within the tropical North Atlantic and Caribbean coincides with near-surface wind intensification describing a southward shift of moisture convergence and convection strengthening over South America (Fig. 5a, b). Similar but less pronounced responses are seen for the YD minus Early Holocene (not shown).

Comparing the iTRACE transient simulations with and without meltwater forcing allows isolation of the AMOC forcing (Fig. 6) on Central American rainfall. We find significant decoupling between simulated $\delta^{18}O_p$ and precipitation in the experiment without meltwater forcing (Fig. 6b, c). Furthermore, the stalagmite $\delta^{18}O$ and iTRACE no meltwater results (black in Fig. 6) are strongly different, demonstrating that the variability observed in speleothem $\delta^{18}O$ data is best explained by the AMOC slowdown associated with meltwater forcing in the North Atlantic.

Atlantic mean state control on rainfall

Given the temporal dissimilarity between Central America and other tropical monsoon regions more strongly paced by orbital precession (Supplementary Fig. 7), we posit that the Central American monsoon represents a thermally-controlled monsoon, distinct from the Global Monsoon. Central America may be distinguished from other monsoon regions because of its physiography of a small and narrow isthmus bounded by a major ocean heat reservoir whose energy budget drives regional convection[31]. We propose that AMOC intensity, tropical Atlantic SST, and northern hemisphere ice sheet extent were the dominant rainfall controls over Central America during the last 140,000 years BP, enhanced by Central America's proximity to the AMOC center of action. For instance, the positive $\delta^{18}O_{ivc}$ excursions between late MIS 4 and MIS 2 (~65,000–17,000 yr BP) occurred coevally with Laurentide Ice sheet expansion and AMOC shifting to a weak glacial circulation mode[13,17], which suppressed Caribbean and Central American atmospheric convection. Furthermore, the lack of clear DO events in our record suggests that Central American paleoclimate differs from that inferred from the Cariaco Basin and the two regions should be viewed as distinct climate regions. Hydroclimate observations in the Caribbean and Central American regions can be now understood as a predominantly thermodynamic response to changing Atlantic Ocean thermal states, and our study thus reconciles previous regional hydroclimate interpretations from the Bahamas[48], Cuba[9,49], Puerto Rico[50], Costa Rica[8], Mexico[10,46,51], and Guatemala[7]

https://doi.org/10.1038/s41467-024-54856-0

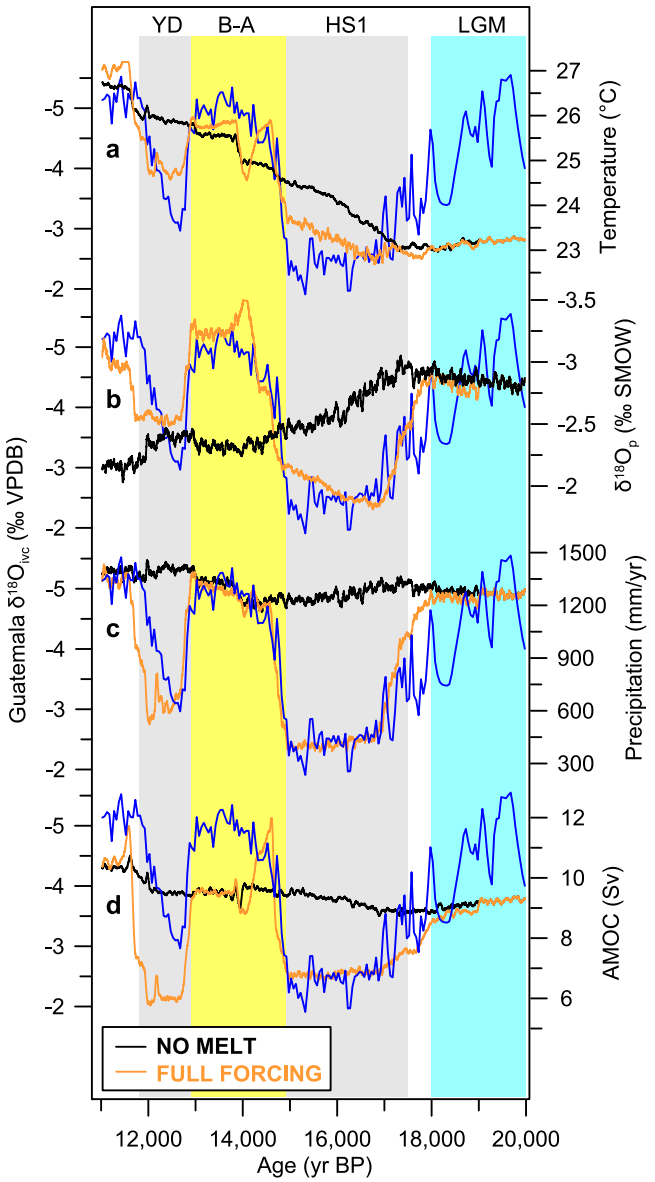

Fig. 6 | Guatemala $\delta^{18}O_{ivc}$ versus iTRACE full forcing and no meltwater forcing results. The Guatemala $\delta^{18}O_{ivc}$ record is shown in blue, and iTRACE full forcing (in orange) and no meltwater forcing as 31-yr averages. **a** iTRACE surface temperature. **b** iTRACE $\delta^{18}O_p$ for MJJASON. **c** iTRACE MJJASON rainfall amount. **d** Simulated AMOC. The remarkable difference between our speleothem $\delta^{18}O_{ivc}$ and the NO MELT experiment results pinpoints the dominant role of AMOC in driving Central American monsoon intensity during the last deglaciation. Vertical bars define Younger Dryas (YD), Bølling-Allerød (B-A), Heinrich Stadial 1 (HS1), and Last Glacial Maximum (LGM).

(Supplementary Fig. 8), which can now be considered a unified regional Central American and Caribbean monsoon system driven primarily by Atlantic Ocean processes.

A bimodal speleothem $\delta^{18}O_{ivc}$ distribution (Supplementary Fig. 9) supports the existence of two main monsoon states, and further implicates the existence of an SST threshold below which widespread atmospheric convection is diminished, possibly related to an SST threshold of ~27 °C that sustains vigorous convection today[12,52,53]. Considered in relation to the background climate boundary conditions, temperature thresholds within the tropical North Atlantic basin might have been lower than modern during intervals of larger/intermediate Northern Hemisphere ice sheets[54] and could potentially increase under future greenhouse warming[53,55].

The Central American paleoclimatic record and data-model comparison have implications for future projections of AMOC, Tropical North Atlantic/Caribbean SST, and monsoon changes. The analysis of different model simulations during the last deglaciation isolates AMOC as a dominant forcing mechanism of regional monsoon convection. Further, Tropical North Atlantic/Caribbean SST was tied to AMOC strength variations throughout the last glacial cycle, triggering rapid transitions in the Central American monsoon convection.

Observational and proxy data suggest that AMOC has weakened over the last century[56–58] in response to increasing greenhouse gas concentrations, while other studies argue that the observed AMOC slowdown results from its internal variability[24,59]. Under various future warming scenarios, AMOC is very likely to weaken by the end of the century[60], although large uncertainties among models hamper our ability to confidently estimate the temporal rates of decline[22,25]. Such a discrepancy has been attributed to the over-stability of AMOC in model simulations[61] and the lack of dynamical cryosphere (i.e., ice melting) and deepwater formation processes[25]. Early-warning signals of AMOC approaching a tipping point are also found in most recent climate models[62,63].

The speleothem data indicate that AMOC weakening alone can trigger widespread reduction of monsoon convection in Central America and the Caribbean, independently of the background thermal conditions. Future rainfall in Central America and the Caribbean is projected to decrease significantly by the end of the century[64–66], but few studies have focused on the role of AMOC[22,67,68]. Whether monsoon regimes weaken in the future will also depend on the direct response to SST warming[69]. However, separating the competing effects of direct radiative, SST warming, and dynamic forcing on future monsoon variations remains challenging[70–74].

In this context, our results stress that if the AMOC- Central American monsoon link documented over the last 140,000 yr BP holds under future warming scenarios, a potential AMOC slowdown or collapse as suggested by climate models[23,62,64–68,75] will likely weaken monsoon convection in Central America and impact freshwater availability in the region.

Methods

Cave sites

The stalagmites were collected from three caves located in the Alta Verapaz Department on the Caribbean slope of Guatemala. Grutas del Rey Marcos (RM) is a private-owned touristic cave located at about 20 km from the city of Cobán (15.427°N and −90.280°W, 1460 m asl). The cave is characterized by a small (gated) entrance into a narrow passage that opens to a sequence of larger rooms highly decorated in speleothems of vadose origin (stalactites, stalagmites, flowstones, draperies, etc.). Bedrock thickness above the cave is about 80–100 m. All samples were retrieved at about 50-70 m from the cave entrance and 'dead-and-down', meaning that no active and/or standing stalagmites were collected for cave preservation reasons. Cave monitoring indicates that relative humidity is nearly 100% year-around and temperature is 17 ± 0.5 °C (Ref. 76). Bombil Pek and Jul Iq caves are located near Chisec, 45 km from Cobán (15.837 °N and −90.277 °W, elevation 240 m asl). The caves open to the surface through a series of sinkholes, and are characterized by a sequence of extensive, highly-decorated conduits and chambers. Bedrock thickness above the caves is between 40–60 m. Stalagmites from BO and JQ caves were collected between 150–200 m from the cave entrance, in sections that had no perceptible airflow.

^{230}Th dating. Seven new stalagmites from Grutas del Rey Marcos (GU-RM-4, −10, −11, and −35), Jul Iq Cave (GU-JQ-2 and −3), and Bombil Pek Cave (GU-BO-1) were analyzed in this study. Two additional ages were determined on stalagmite GU-RM-1 (ref. 12). The stalagmites consisted of columnar and open compact calcite; no aragonite was observed.

^{230}Th radiometric dating was performed at the Isotope Laboratory facilities of the Institute of Global Environmental Change, Xi'an Jiaotong University. Sub-samples of ~60–150 mg were drilled along the growth axis using a SHERLINE 5410 milling device in clear compact calcite layers whenever possible. Uranium and thorium separation followed the standard chemical procedures described in ref. 77. A triple-spike ^{229}Th-^{233}U-^{236}U isotope dilution method was applied to monitor U-Th concentrations and isotope ratios and correct for instrumental fractionation effects. U/Th isotopic ratios were measured on a Thermo-Finnigan Neptune multi-collector inductively coupled plasma mass spectrometer (MC-ICP-MS) using updated techniques described in ref. 58. All ages were calculated using half-lives from refs. 78–80, and corrected for detrital contamination using a ^{230}Th/^{232}Th atomic ratio of 4.4 ppm, assuming secular equilibrium with a bulk earth ^{232}Th/^{238}U value of 3.8 (Ref. 81). All age uncertainties are reported as absolute 2σ and include analytical errors and initial ^{230}Th/^{232}Th ratio. Age corrections are relatively small (~ 20–100 years) for samples with moderate uranium concentration and little ^{232}Th contents, while samples having higher concentrations of detrital thorium (i.e., ^{232}Th > 1000 ppt) and/or low uranium content are more susceptible to ^{230}Th/^{232}Th correction (~300–1500 years) and exhibit larger age uncertainties. All data are shown in Supplementary Table 1.

Stable isotope analysis. Oxygen and carbon isotope measurements were done at the Las Vegas Isotope Science Laboratory (LVIS) of the University of Nevada Las Vegas, Las Vegas (USA). Sub-samples were drilled/milled along the stalagmite growth axes at intervals between 0.2 and 1 mm, producing a subset of 3169 isotope analyses for the stalagmites used here. Sample powders were reacted with 104% phosphoric acid at 70 °C in a Kiel IV automated carbonate preparation device, the CO_2 gas was separated via cryogenic trapping, and isotope measurements were performed on a ThermoElectron Delta V Plus isotope ratio mass spectrometer in dual inlet mode. Isotope values were corrected with an internal standard (USC-1) and reported as δ-‰ deviations from the Vienna Pee Dee Belemnite (VPDB) standard scale. USC-1 values were previously determined by calibration with international standards NBS-18 and NBS-19. Analytical uncertainties are 0.03–0.05 ‰ for δ^{13}C and 0.08–0.11 ‰ for δ^{18}O. Cave and rainwater isotope analyses (Supplementary Tables 4–5) were completed at the Center for Stable Isotopes (CSI) of the University of New Mexico (Albuquerque, NM) using a cavity ring-down spectroscopy L1102-I Water Isotopic Analyzer bracketed with calibrated internal standards. δ^2H and δ^{18}O precision are better than ± 2.0 ‰ and 0.06 ‰, respectively. Because the speleothems were collected from three different cave systems with potentially unique hydrology and vegetation cover the δ^{13}C analyses are not discussed further here.

Age modeling. Individual stalagmite age models were constructed using the COPRA algorithm[82], which employs Monte-Carlo age model simulations (n = 2000) that can constrain uncertainties in both the time and proxy space. ^{230}Th age outliers with high detrital thorium and ages significantly older than the age/depth trends from cleaner samples were omitted from the final age models (Grey shading in Table S1 indicates excluded dates). In cases where poorly-dated sections of stalagmites were compromised by detrital ^{230}Th but had similar δ^{18}O profiles to well-dated stalagmites, we tuned small sections of the stalagmites to the better-dated stalagmites to provide greater time coverage; the δ^{18}O data from the base of GU-RM-1 and GU-RM-35 were tuned to the better chronologies of GU-RM-10 and GU-RM-11 using tie-points on clearly correlative δ^{18}O anomalies across the interval 14-10.5 kyr BP (see Supplementary Fig. 10). The age tie points assume ±200 years uncertainty and were subsequently used in the final COPRA age model. Age model uncertainty and age resolution varies among the different stalagmites, and are about ±200–600 years and ±11-221 years at the 95% confidence interval, respectively.

Guatemala composite δ^{18}O record. Stalagmite δ^{18}O values were composited by binning into 50-yr average bins. Prior to compositing, stalagmites δ^{18}O for BO and JQ caves were adjusted by −0.6 ‰ relative to RM, to account for different temperature-dependent equilibrium fractionation based on their lower elevation and higher temperatures relative to RM cave, and assuming that modern water-calcite equilibrium conditions were similar during the last glacial cycle. Despite BO and JQ caves being virtually at the same elevation, a further 0.4 ‰ correction to the JQ samples was applied to align absolute values, which differed slightly between coeval stalagmites while sharing the same overall structure. The origin of the small offsets is not clear, but soil and/or epikarst processes (i.e., PCP[83]) may have a small influence on the δ^{18}O of drips feeding the different stalagmite sites while preserving the overall replication and time series structure between stalagmites. Because the fractionation of isotopes in precipitation is relative to the ocean δ^{18}O value, and because the ocean δ^{18}O itself has changed, we corrected composite Guatemala (GUA) δ^{18}O record for the δ^{18}O of the ocean from global ice-volume variations to create a $\delta^{18}O_{ivc}$ record using the Waelbroeck, et al.[32] reconstruction. The ice-volume correction accounts for up to 1–1.2 ‰ decrease (more negative) in speleothem δ^{18}O values during the glacial periods (i.e., LGM, MIS, 4, and MIS 6) and is relatively small for interglacial stages (i.e., Holocene, MIS 5). This correction does not influence the interpretations or change the δ^{18}O time series in any substantial way.

iTRACE transient climate ensemble simulations. We use the iTRACE[47] model output to support the dynamical interpretation of reconstructed Guatemalan rainfall changes. iTRACE is, to our knowledge, the only publicly available transient climate simulation ensemble with a model that incorporates oxygen-isotopes within the ocean, atmosphere, land surface, and sea-ice allowing to directly compare precipitation and temperature simulations with proxy records. The model is built in the Community Earth System Model CESM v.1.3, with a land and atmosphere spatial resolution of 1.9° and 2.5° (latitude and longitude), and a nominal 1°resolution for the ocean and sea ice[84]. CESM simulations have been successfully validated against modern observations of rainfall variations across the global tropics[85,86]. Previous studies have shown that the CESM model ensemble reproduces the overall precipitation variability in Central America and the Caribbean in both modern and paleoclimate timescales[10,64,87]. However, biases in the estimate of magnitude and rate of seasonal rainfall changes were noticed, particularly for the early-wet season (May-June), possibly related to the low spatial resolution of the models that lack of reliably capture the complex regional topography and divergence in modeling regional SST variations[88–90]. Although the iTRACE model ensemble only simulates the last deglaciation (20-11 kyr BP), it provides a direct means for testing regional climate dynamics during abrupt millennial-scale dry intervals such as Heinrich stadial 1 (HS1) and Younger Dryas (YD). iTRACE includes a full-forcing experiment with ice sheets, greenhouse gases, orbital, and meltwater forcing related to ice dynamics into the high latitude oceans, as well as sensitivity experiments where some of the forcings are neglected. We extracted seasonal (DJFMA, MJJ, and ASON) precipitation, surface temperature, wind fields at 200 hPa (upper level) and 1000 hPa (surface), and oxygen isotopes for both convective and large-scale rainfall. The AMOC strength (in Sverdrups -Sv) is obtained from the zonally-integrated meridional overturning transport in the Atlantic Ocean, including its Eulerian mean, eddy-induced, and sub-mesoscale components, averaged over the domain encompassing 500–1200 meters depth from the equator to 49.6°N latitude. Spatially-averaged time series for the Caribbean and Central American region were extracted between 1010.4° and 21.88° latitude, and 265° to 300° longitude to emphasize regional climatic processes.

Simulated $\delta^{18}O_p$ is calculated as follows:

$$\delta^{18}O_p = \left[\left(\frac{Pr_{180}}{Pr_{160}}\right) - 1\right] \times 1000 \quad (1)$$

where Pr_{18O} and Pr_{16O} are the sum of convective and large-scale rainfall amounts for $H_2{}^{18}O$ and $H_2{}^{16}O$, respectively. Local atmospheric convective activity is estimated from the horizontal wind fields as the difference between upper level (200 hPa) and lower level (1000 hPa) divergence. Specifically, given the velocity vector field **V** and its horizontal u and v components along the zonal and meridional axes identified by x and y, respectively, the horizontal divergence (∇_H) of **V** is defined as:

$$\nabla_H \cdot \mathbf{V} = \frac{\partial u}{\partial x} + \frac{\partial v}{\partial y} \quad (2)$$

A convective activity index is calculated from the horizontal divergence at 200 hPa and 1000 hPa as:

$$(\nabla_H \cdot \mathbf{V})_{200} - (\nabla_H \cdot \mathbf{V})_{1000} \quad (3)$$

where positive and negative anomalies of the index indicate enhanced and reduced atmospheric convection, respectively. Values of a variable in two periods are considered to be significantly different if the corresponding distributions do not overlap within the 1-99 percentile range

Data availability

Speleothem stable isotope data produced in the study are available from the NOAA World Data Service for Paleoclimatology at: https://www.ncei.noaa.gov/access/paleo-search/study/39960. Source data are provided with this paper.

References

1. Wang, P. X. et al. The global monsoon across timescales: coherent variability of regional monsoons. *Climate* **10**, 2007–2052 (2014).
2. Cheng, H. et al. The Asian monsoon over the past 640,000 years and ice age terminations. *Nature* **534**, 640–646 (2016).
3. Wang, X. et al. Wet periods in northeastern Brazil over the past 210 kyr linked to distant climate anomalies. *Nature* **432**, 740–743 (2004).
4. Mohtadi, M., Prange, M. & Steinke, S. Palaeoclimatic insights into forcing and response of monsoon rainfall. *Nature* **533**, 191–199 (2016).
5. Geen, R., Bordoni, S., Battisti, D. S. & Hui, K. Monsoons, ITCZs, and the Concept of the Global Monsoon. *Rev. Geophys.* **58**, https://doi.org/10.1029/2020rg000700 (2020).
6. Wang, B. & Ding, Q. Global monsoon: Dominant mode of annual variation in the tropics. *Dyn. Atmos. Oceans* **44**, 165–183 (2008).
7. Hodell, D. A. et al. An 85-ka record of climate change in lowland Central America. *Quat. Sci. Rev.* **27**, 1152–1165 (2008).
8. Lachniet, M. S. et al. Late Quaternary moisture export across Central America and to Greenland: evidence for tropical rainfall variability from Costa Rican stalagmites. *Quat. Sci. Rev.* **28**, 3348–3360 (2009).
9. Warken, S. F. et al. Caribbean hydroclimate and vegetation history across the last glacial period. *Quat. Sci. Rev.* **218**, 75–90 (2019).
10. Wright, K. T. et al. Dynamic and thermodynamic influences on precipitation in Northeast Mexico on orbital to millennial timescales. *Nat. Commun.* **14**, https://doi.org/10.1038/s41467-023-37700-9 (2023).
11. Dawson, R. R. et al. Zonal control on Holocene precipitation in northwestern Madagascar based on a stalagmite from Anjohibe. *Sci. Rep.* **14**, 5496 (2024).
12. Winter, A. et al. Initiation of a stable convective hydroclimatic regime in Central America circa 9000 years BP. *Nat. Commun.* **11**, 716 (2020).
13. Henry, L. G. et al. North Atlantic ocean circulation and abrupt climate change during the last glaciation. *Science* **353**, 470–474 (2016).
14. Peterson, L. C. Rapid changes in the hydrologic cycle of the Tropical Atlantic during the last glacial. *Science* **290**, 1947–1951 (2000).
15. Deplazes, G. et al. Links between tropical rainfall and North Atlantic climate during the last glacial period. *Nat. Geosci.* **6**, 213–217 (2013).
16. Lenton, T. M. et al. Tipping elements in the Earth's climate system. *Proc. Natl Acad. Sci.* **105**, 1786–1793 (2008).
17. Bohm, E. et al. Strong and deep Atlantic meridional overturning circulation during the last glacial cycle. *Nature* **517**, 73–76 (2015).
18. Bradley, R. S. & Diaz, H. F. Late quaternary abrupt climate change in the tropics and sub-tropics: the continental signal of tropical hydroclimatic events (THEs). *Rev. Geophys.* **59**, e2020RG000732 (2021).
19. Frierson, D. M. W. et al. Contribution of ocean overturning circulation to tropical rainfall peak in the Northern Hemisphere. *Nat. Geosci.* **6**, 940–944 (2013).
20. Yu, S. & Pritchard, M. S. A strong role for the AMOC in partitioning global energy transport and shifting ITCZ position in response to latitudinally discrete solar forcing in CESM1.2. *J. Clim.* **32**, 2207–2226 (2019).
21. Weijer, W., Cheng, W., Garuba, O. A., Hu, A. & Nadiga, B. T. CMIP6 Models Predict Significant 21st Century Decline of the Atlantic Meridional Overturning Circulation. *Geophys. Res. Lett.* **47**, https://doi.org/10.1029/2019gl086075 (2020).
22. Bellomo, K., Angeloni, M., Corti, S. & Von Hardenberg, J. Future climate change shaped by inter-model differences in Atlantic meridional overturning circulation response. *Nat. Commun.* **12**, https://doi.org/10.1038/s41467-021-24015-w (2021).
23. Bellomo, K. & Mehling, O. Impacts and State-Dependence of AMOC Weakening in a Warming Climate. *Geophys. Res. Lett.* **51**, https://doi.org/10.1029/2023gl107624 (2024).
24. Kilbourne, K. H. et al. Atlantic circulation change still uncertain. *Nat. Geosci.* **15**, 165–167 (2022).
25. McCarthy, G. D. & Caesar, L. Can we trust projections of AMOC weakening based on climate models that cannot reproduce the past? *Philos. Trans. Royal Soc. A: Math. Phys. Eng. Sci.* **381**, https://doi.org/10.1098/rsta.2022.0193 (2023).
26. Wang, C., Enfield, D. B., Lee, S.-K. & Landsea, C. W. Influences of the Atlantic Warm Pool on Western Hemisphere Summer Rainfall and Atlantic Hurricanes. *J. Clim.* **19**, 3011–3028 (2006).
27. Wang, C. Variability of the Caribbean Low-Level Jet and its relations to climate. *Clim. Dyn.* **29**, 411–422 (2007).
28. Wang, C. & Lee, S.-k. Atlantic warm pool, Caribbean low-level jet, and their potential impact on Atlantic hurricanes. *Geophys. Res. Lett.* **34**, https://doi.org/10.1029/2006GL028579 (2007).
29. Martinez, C., Goddard, L., Kushnir, Y. & Ting, M. Seasonal climatology and dynamical mechanisms of rainfall in the Caribbean. *Clim. Dyn.* **53**, 825–846 (2019).
30. Bardales, W. A., Campos, L., Gómez, R., Ordóñez, S. & Machuca, N. Variabilidad y Cambio Climatico en Guatemala. 147 (Instituto Nacional de Sismología, Vulcanología, Meteorología e Hidrología, 2019).
31. Wang, C. & Enfield, D. B. A further study of the tropical western hemisphere Warm Pool. *J. Clim.* **16**, 1476–1493 (2003).
32. Waelbroeck, C. et al. Sea-level and deep water temperature changes derived from benthic foraminifera isotopic records. *Quat. Sci. Rev.* **21**, 295–305 (2002).
33. Lachniet, M. S. & Patterson, W. P. Oxygen isotope values of precipitation and surface waters in northern Central America (Belize and Guatemala) are dominated by temperature and amount effects. *Earth Planet. Sci. Lett.* **284**, 435–446 (2009).
34. Durán-Quesada, A. M., Gimeno, L., Amador, J. A. & Nieto, R. Moisture sources for Central America: Identification of moisture sources using a Lagrangian analysis technique. *J. Geophys. Res.* **115**, https://doi.org/10.1029/2009jd012455 (2010).

35. Hemming, S. R. Heinrich events: Massive late Pleistocene detritus layers of the North Atlantic and their global climate imprint. *Rev.Geophys.* **42**, https://doi.org/10.1029/2003rg000128 (2004).
36. Martrat, B. et al. Four climate cycles of recurring deep and surface water destabilizations on the Iberian margin. *Science* **317**, 502–507 (2007).
37. Cruz, F. W. et al. Insolation-driven changes in atmospheric circulation over the past 116,000 years in subtropical Brazil. *Nature* **434**, 63–66 (2005).
38. Carolin, S. A. et al. Varied response of Western Pacific hydrology to climate forcings over the last glacial period. *Science* **340**, 1564–1566 (2013).
39. Rama-Corredor, O. et al. Parallelisms between sea surface temperature changes in the western tropical Atlantic (Guiana Basin) and high latitude climate signals over the last 140,000 years. *Climate* **11**, 1297–1311 (2015).
40. Andersen, K. K. et al. High-resolution record of Northern Hemisphere climate extending into the last interglacial period. *Nature* **431**, 147–151 (2004).
41. Heinrich, H. Origin and consequences of cyclic ice rafting in the northeast Atlantic Ocean during the past 130,000 years. *Quat. Res.* **29**, 142–152 (1988).
42. Lisiecki, L. E. & Stern, J. V. Regional and global benthic δ18O stacks for the last glacial cycle. *Paleoceanography* **31**, 1368–1394 (2016).
43. Rasmussen, S. O. et al. A stratigraphic framework for abrupt climatic changes during the Last Glacial period based on three synchronized Greenland ice-core records: refining and extending the INTIMATE event stratigraphy. *Quat. Sci. Rev.* **106**, 14–28 (2014).
44. Ramirez, V. M. et al. Summer insolation controlled movements of Intertropical Convergence Zone during last glacial cycle in northern South America. *Commun. Earth Environ.* **4**, https://doi.org/10.1038/s43247-023-01124-6 (2023).
45. McManus, J. F., Francois, R., Gherardi, J. M., Keigwin, L. D. & Brown-Leger, S. Collapse and rapid resumption of Atlantic meridional circulation linked to deglacial climate changes. *Nature* **428**, 834–837 (2004).
46. Lachniet, M. S., Asmerom, Y., Bernal, J. P., Polyak, V. J. & Vazquez-Selem, L. Orbital pacing and ocean circulation-induced collapses of the Mesoamerican monsoon over the past 22,000 y. *Proc. Natl Acad. Sci. USA* **110**, 9255–9260 (2013).
47. He, C. et al. Deglacial variability of South China hydroclimate heavily contributed by autumn rainfall. *Nat. Commun.* **12**, 5875 (2021).
48. Arienzo, M. M. et al. Multi-proxy evidence of millennial climate variability from multiple Bahamian speleothems. *Quat. Sci. Rev.* **161**, 18–29 (2017).
49. Ait Brahim, Y. et al. Hydroclimate variability in the Caribbean during North Atlantic Heinrich cooling events (H8 and H9). *Sci. Rep.* **12**, https://doi.org/10.1038/s41598-022-24610-x (2022).
50. Warken, S. F. et al. Persistent Link Between Caribbean Precipitation and Atlantic Ocean circulation during the last glacial revealed by a Speleothem Record From Puerto Rico. *Paleoceanogr. Paleoclimatol.* **35**, https://doi.org/10.1029/2020pa003944 (2020).
51. Travis-Taylor, L. et al. Last glacial hydroclimate variability in the Yucatán Peninsula not just driven by ITCZ shifts. *Sci. Rep.* **13**, https://doi.org/10.1038/s41598-023-40108-6 (2023).
52. Graham, N. E. & Barnett, T. P. Sea surface temperature, surface wind divergence, and convection over Tropical Oceans. *Science* **238**, 657–659 (1987).
53. Johnson, N. C. & Xie, S.-P. Changes in the sea surface temperature threshold for tropical convection. *Nat. Geosci.* **3**, 842–845 (2010).
54. Hodell, D. A. et al. Late Glacial temperature and precipitation changes in the lowland Neotropics by tandem measurement of δ18O in biogenic carbonate and gypsum hydration water. *Geochim. Cosmochim. Acta* **77**, 352–368 (2012).
55. Xie, S.-P. et al. Global warming pattern formation: sea surface temperature and rainfall. *J. Clim.* **23**, 966–986 (2010).
56. Caesar, L., McCarthy, G. D., Thornalley, D. J. R., Cahill, N. & Rahmstorf, S. Current Atlantic Meridional Overturning Circulation weakest in last millennium. *Nat. Geosci.* **14**, 118–120 (2021).
57. Boers, N. Observation-based early-warning signals for a collapse of the Atlantic Meridional Overturning Circulation. *Nat. Clim. Change* **11**, 680–688 (2021).
58. Rahmstorf, S. et al. Exceptional twentieth-century slowdown in Atlantic Ocean overturning circulation. *Nat. Clim. Change* **5**, 475–480 (2015).
59. Latif, M., Sun, J., Visbeck, M. & Hadi Bordbar, M. Natural variability has dominated Atlantic Meridional Overturning Circulation since 1900. *Nat. Clim. Change* **12**, 455–460 (2022).
60. IPCC. *Climate Change 2021: The Physical Science Basis. Contribution of Working Group I to the Sixth Assessment Report of the Intergovernmental Panel on Climate Change*. Vol. In Press (Cambridge University Press, 2021).
61. Liu, W., Xie, S.-P., Liu, Z. & Zhu, J. Overlooked possibility of a collapsed Atlantic Meridional Overturning Circulation in warming climate. *Sci. Adv.* **3**, e1601666 (2017).
62. Ditlevsen, P. & Ditlevsen, S. Warning of a forthcoming collapse of the Atlantic meridional overturning circulation. *Nat. Commun.* **14**, 4254 (2023).
63. van Westen, R. M., Kliphuis, M. & Dijkstra, H. A. Physics-based early warning signal shows that AMOC is on tipping course. *Sci. Adv.* **10**, eadk1189 (2024).
64. Almazroui, M. et al. Projected Changes in Temperature and Precipitation Over the United States, Central America, and the Caribbean in CMIP6 GCMs. *Earth Syst. Environ.* **5**, 1–24 (2021).
65. Durán-Quesada, A. M., Sorí, R., Ordoñez, P. & Gimeno, L. Climate perspectives in the Intra–Americas Seas. *Atmosphere* **11**, https://doi.org/10.3390/atmos11090959 (2020).
66. Imbach, P. et al. Future climate change scenarios in Central America at high spatial resolution. *PLoS One* **13**, e0193570 (2018).
67. Chen, Y., Langenbrunner, B. & Randerson, J. T. Future drying in Central America and Northern South America linked With Atlantic Meridional OVERTURNING CIRCulation. *Geophys. Res. Lett.* **45**, 9226–9235 (2018).
68. Orihuela-Pinto, B., England, M. H. & Taschetto, A. S. Interbasin and interhemispheric impacts of a collapsed Atlantic Overturning Circulation. *Nat. Clim. Change* **12**, 558–565 (2022).
69. Pascale, S., Carvalho, L. M. V., Adams, D. K., Castro, C. L. & Cavalcanti, I. F. A. Current and future variations of the monsoons of the Americas IN A WARMING CLImate. *Curr. Clim. Change Rep.* **5**, 125–144 (2019).
70. Chen, Z. et al. Global land monsoon precipitation changes in CMIP6 projections. *Geophys. Res. Lett.* **47**, e2019GL086902 (2020).
71. Ha, K.-J., Kim, B.-H., Chung, E.-S., Chan, J. C. & Chang, C.-P. Major factors of global and regional monsoon rainfall changes: Natural versus anthropogenic forcing. *Environ. Res. Lett.* **15**, 034055 (2020).
72. Long, S.-M., Xie, S.-P. & Liu, W. Uncertainty in tropical rainfall projections: Atmospheric circulation effect and the ocean coupling. *J. Clim.* **29**, 2671–2687 (2016).
73. Seth, A. et al. Monsoon responses to climate changes—connecting past, present and future. *Curr. Clim. Change Rep.* **5**, 63–79 (2019).
74. Pascale, S. et al. Weakening of the North American monsoon with global warming. *Nat. Clim. Change* **7**, 806–812 (2017).
75. Lohmann, J. & Ditlevsen, P. D. Risk of tipping the overturning circulation due to increasing rates of ice melt. *Proc. Natl Acad. Sci.* **118**, e2017989118 (2021).
76. Bernal, J. P. et al. Variability of trace-elements and δ18O in drip water from Gruta del Rey Marcos, Guatemala; seasonal and

environmental effects, and its implications for paleoclimate reconstructions. *Front. Earth Sci.* **11**, 1–16 (2023).
77. Cheng, H. et al. Improvements in 230Th dating, 230Th and 234U half-life values, and U–Th isotopic measurements by multi-collector inductively coupled plasma mass spectrometry. *Earth Planet. Sci. Lett.* **371-372**, 82–91 (2013).
78. Jaffey, A., Flynn, K., Glendenin, L., Bentley, W. T. & Essling, A. Precision measurement of half-lives and specific activities of U 235 and U 238. *Phys. Rev. C.* **4**, 1889 (1971).
79. Cheng, H. et al. The half-lives of uranium-234 and thorium-230. *Chem. Geol.* **169**, 17–33 (2000).
80. Edwards, R. L., Chen, J. & Wasserburg, G. 238U234U230Th232Th systematics and the precise measurement of time over the past 500,000 years. *Earth Planet. Sci. Lett.* **81**, 175–192 (1987).
81. Richards, D. A. & Dorale, J. A. Uranium-series chronology and environmental applications of speleothems. *Rev. Mineral. Geochem.* **52**, 407–460 (2003).
82. Breitenbach, S. F. M. et al. COnstructing Proxy Records from Age models (COPRA). *Climate* **8**, 1765–1779 (2012).
83. Patterson, E. W. et al. Local hydroclimate alters interpretation of speleothem δ18O records. *Nat. Commun.* **15**, https://doi.org/10.1038/s41467-024-53422-y (2024).
84. He, C. et al. Hydroclimate footprint of pan-Asian monsoon water isotope during the last deglaciation. *Sci. Adv.* **7**, eabe2611 (2021).
85. Brady, E. et al. The connected isotopic water cycle in the Community Earth System Model version 1. *J. Adv. Model. Earth Syst.* **11**, 2547–2566 (2019).
86. Kay, J. E. et al. The Community Earth System Model (CESM) large ensemble project: A community resource for studying climate change in the presence of internal climate variability. *Bull. Am. Meteorol. Soc.* **96**, 1333–1349 (2015).
87. Bhattacharya, T. & Coats, S. Atlantic-Pacific Gradients Drive Last Millennium Hydroclimate Variability in Mesoamerica. *Geophys. Res. Lett.* **47**, https://doi.org/10.1029/2020gl088061 (2020).
88. Garcia-Martinez, I. M. *Mechanisms of Climate Variation in the Broader Mexican-United States Region: The Role of Atmospheric Circulation and Anthropogenic Forcing*. PhD thesis, University of Edinburgh (2020).
89. Pascale, S., Kapnick, S. B., Delworth, T. L., Hidalgo, H. G. & Cooke, W. F. Natural variability vs forced signal in the 2015–2019 Central American drought. *Clim. Change* **168**, https://doi.org/10.1007/s10584-021-03228-4 (2021).
90. Baldwin, J. W., Atwood, A. R., Vecchi, G. A. & Battisti, D. S. Outsize Influence of Central American Orography on Global Climate. *AGU Adv.* **2**, https://doi.org/10.1029/2020av000343 (2021).
91. Berger, A. & Loutre, M. F. Insolation values for the climate of the last 10 million years. *Quat. Sci. Rev.* **10**, 297–317 (1991).
92. Pawlowicz, R. M_Map: a mapping package for MATLAB, version 1.4m. www.eoas.ubc.ca/~rich/map.html (2020).
93. Wessel, P. & Smith, W. H. A global, self-consistent, hierarchical, high-resolution shoreline database. *J. Geophys. Res.: Solid Earth* **101**, 8741–8743 (1996).

Acknowledgements

We thank the Fernandez family (Grutas del Rey Marcos) and the Asociación Bombil Pek el Por Venir (Bombil Pek and Juliq caves) for permitting cave access and sampling, B.P. Onac and F. Revolorio for helping with fieldwork, V. Atudorei at the Center of Stable Isotopes of the University of New Mexico for providing laboratory facilities for water isotope analyses, and J. Xue from the Radiogenic Laboratory facilities of Xi'an Jiaotong University for the U-series analyses. Collaborative National Science Foundation (NSF) research grant AGS 1804263 to M.S.L. and A.W. funded the study. G.L was supported by the NSF grant AGS 1804263, University of Nevada Top-tier doctoral graduate research assistantship (TTDGRA), and the Geology Society of America Graduate Student Research grant. M.S.L. and A.W. are grateful for Visiting Scholar support at Università Ca' Foscari Venezia.

Author contributions

M.S.L. and A.W. designed the research; G.L., M.S.L., A.W., M.X., and D.Z. conducted fieldwork; O.V. contributed to rainfall sampling. G.L. and M.S.L. conducted the stable isotope measurements; H.C. performed the ^{230}Th dating analysis. G.L. and M.S.L wrote the manuscript; D.Z. carried the iTRACE model analysis and contributed to the discussion of data-model comparison. A.R. and J.P.B. contributed to the discussion of results and the final draft of the manuscript.

Competing interests

The authors declare no competing interests.

Additional information

Supplementary information The online version contains supplementary material available at https://doi.org/10.1038/s41467-024-54856-0.

Correspondence and requests for materials should be addressed to Matthew S. Lachniet.

Peer review information *Nature Communications* thanks Matthew Schmidt, Benjamin Tiger, and the other, anonymous, reviewer(s) for their contribution to the peer review of this work. A peer review file is available.